



## The cationic interstitials induced resistive switching: a case study on Mn-doped SnO<sub>2</sub>

Zhemi Xu, Tianhao Ji, Shule Zhang, Peiyuan Guan, Joshua Elliott, Tao Wan, Claudio Cazorla & Dewei Chu

**To cite this article:** Zhemi Xu, Tianhao Ji, Shule Zhang, Peiyuan Guan, Joshua Elliott, Tao Wan, Claudio Cazorla & Dewei Chu (2023) The cationic interstitials induced resistive switching: a case study on Mn-doped SnO<sub>2</sub>, *Materials Science and Technology*, 39:10, 1180-1186, DOI: 10.1080/02670836.2022.2163533

**To link to this article:** <https://doi.org/10.1080/02670836.2022.2163533>



Published online: 05 Jan 2023.



Submit your article to this journal [↗](#)



Article views: 170



View related articles [↗](#)



View Crossmark data [↗](#)



# The cationic interstitials induced resistive switching: a case study on Mn-doped SnO<sub>2</sub>

Zhemi Xu<sup>a</sup>, Tianhao Ji<sup>a</sup>, Shule Zhang<sup>a</sup>, Peiyuan Guan <sup>b</sup>, Joshua Elliott<sup>c</sup>, Tao Wan<sup>b</sup>, Claudio Cazorla<sup>d</sup> and Dewei Chu<sup>b</sup>

<sup>a</sup>Chemistry and Material Engineering College, Beijing Technology and Business University, Beijing, People's Republic of China; <sup>b</sup>School of Materials Science and Engineering, University of New South Wales, Sydney, Australia; <sup>c</sup>Department of Chemical Engineering and Analytical Science, University of Manchester, Manchester, UK; <sup>d</sup>Departament de Física, Universitat Politècnica de Catalunya, Barcelona, Spain

## ABSTRACT

This work has explored the possible defects in Mn-doped SnO<sub>2</sub> and compared the effects of interstitial Mn and oxygen vacancies on the electronic structure of SnO<sub>2</sub>. Combining the DFT calculations and experimental measurements, we found that when the Mn-doped SnO<sub>2</sub> is synthesised under Sn-rich or O-poor conditions, the defect pair of Mn substitution and interstitial rather than oxygen vacancy will be formed, which induces energy band across the Fermi level and significantly affects the electronic structure of SnO<sub>2</sub>. With the Mn interstitials, stable intrinsic multi-level resistive states and optical SET can be achieved in the Mn-doped SnO<sub>2</sub> memristors. This result can provide guidance in the fabrications of defective metal oxides and promote the investigations on cationic interstitial triggered multi-level resistive switching and optoelectronic memristors.

## ARTICLE HISTORY

Received 8 May 2022  
Revised 27 November 2022  
Accepted 22 December 2022

## KEYWORDS

Tin oxide; defects; cationic interstitials

## Introduction

As one of the most promising candidates for the next generation, memristors have been intensively investigated as they show great potential applications in non-volatile memory, logic operations, and neuromorphic computing [1–4]. The resistive random access memory (RRAM) based on memristors can achieve multi-level resistive switching to multiple data storage densities [5,6], combining data storage and process to realise autonomous learning systems as artificial synapses [7,8], thus, it may conquer the shortcomings of the current von Neumann computer architecture.

Resistive switching (RS) behaviour is realised via the change of internal states under external stimuli, e.g. electric field, magnetic field, light, etc., and the mechanism of resistive switching behaviour is highly associated with the electrodes and materials used in memristors. Among the large variety of materials found to be applicable in RRAM, transition metal oxides have attracted extensive attention owing to their easy fabrication process, good stability and performance, and high compatibility with complementary metal–oxide–semiconductor (CMOS) technology [9,10].

Mechanistic investigations on oxide RRAMs so far mainly focused on the migration of oxygen vacancies (V<sub>O</sub>) from the oxide [11,12] or that of cations from

active electrodes, such as Ag, Cu, and Al [13–15]. However, due to the high mobility of V<sub>O</sub> and the relative low endurance of cation-based RRAMs, it is a challenge to maintain effective intermediate states for RRAMs, which greatly limited the applications of memristors in multi-level RS and artificial synapses.

Cationic interstitials, another common defect in oxides, however, have been overlooked in realising RS, especially in realising multi-level RS and analogue RS [16]. To the best of our knowledge, there are only a few instances that demonstrated the critical role in realising RS: based on the density functional theory (DFT), Zhu et al. compared the V<sub>O</sub> and Ta interstitial in the Ta<sub>2</sub>O<sub>5</sub>-based RRAM and confirmed the contribution of Ta interstitials in realising RS under oxygen-poor conditions [12]. Moreover, both Cu interstitials in Cu/Ta<sub>2</sub>O<sub>5</sub>/Pt [17] and Zr interstitials in CeO<sub>2</sub> [18] also result in RS. Experimentally, by minimising the V<sub>O</sub> effects in the Ta/TaO<sub>x</sub>-based RRAM, the contribution of Ta interstitials in RS has been uncovered for the first time [12]. Following the studies on Sn interstitials in SnO<sub>2</sub>-based RRAM [19], Ti interstitials in TiO<sub>2</sub>-based RRAM [20] and Cu interstitials in Cu<sub>2</sub>O/Al<sub>2</sub>O<sub>3</sub> [21], the contribution of cationic interstitials in RRAM has been confirmed. However, the critical role of cationic interstitials in achieving multi-level RS and synaptic behaviour via light stimuli remains unrevealed.

**CONTACT** Peiyuan Guan  peiyuan.guan@unsw.edu.au  School of Materials Science and Engineering, University of New South Wales, Sydney 2052, Australia; Joshua Elliott  joshua.elliott@diamond.ac.uk  Department of Chemical Engineering and Analytical Science, University of Manchester, Manchester M13 9PL, UK

 Supplemental data for this article can be accessed here. <https://doi.org/10.1080/02670836.2022.2163533>

SnO<sub>2</sub> is a multifunctional wide bandgap semiconductor with various unique properties and high chemical and thermal stability, which has been widely used in many electronic devices [22–24]. Meanwhile, its high transmittance at visible and near-IR wavelengths makes it highly suitable in the light-driven devices compared to various metal oxides [25,26]. In our previous work, superior multi-state RS behaviour has been achieved in Mn-doped SnO<sub>2</sub> RRAM with stable multi-level resistance states and good endurance [27]. By comparing the pure SnO<sub>2</sub> with Mn-, Al-, and In-doped SnO<sub>2</sub>, we found that multi-level RS can be attributed to Mn<sup>3+</sup>. However, there is still a lack of a systematic analysis of Mn-doped SnO<sub>2</sub> that probes the mechanism for intermediate resistance states. The investigation of possible defects and electrical properties of Mn-doped SnO<sub>2</sub> is critical to understanding the underlying mechanisms, such as why Mn-doping improved the resistive states, how Mn-doping contributes to the optimization of SnO<sub>2</sub> electronic properties, and whether such an optimization enables light-controlled resistive switching, etc.

Motivated by these challenges, this paper systematically investigates the structures and electronic properties of Mn-doped SnO<sub>2</sub>, considering all the possible Mn-doping-induced defects. It is found that the co-existence of Mn substitutions at Sn sites with Mn interstitials in SnO<sub>2</sub> superlattice has the highest forming possibility in Mn-doped SnO<sub>2</sub>. It is because of such defects that the Mn-doped SnO<sub>2</sub> becomes an ideal material for multilevel RS devices, which has been further confirmed in experimental studies. Our theoretical and experimental studies provide further insights into how cationic interstitials change the electronic properties of metal oxides, which may shed some light on fabricating memristors through controlled defect engineering.

## Methods

Experimentally, the 12.5 mol-% Mn-doped SnO<sub>2</sub> nanocrystals were synthesised via a liquid–liquid interface solvothermal process and then deposited on a gold-coated Si substrate for electrical characterisations, as illustrated in Figure S-1, and the XRD and XPS characterisations on Mn-doped SnO<sub>2</sub> can be found in Figure S-2 in the ESI. Detailed experimental methods, characterisations of Mn-doped SnO<sub>2</sub> nanocrystals, thin films, and Au/Mn-doped SnO<sub>2</sub>/Au RRAMs can be found in our previous works [27,28].

The formation energy, structure, and other properties of pristine and doped SnO<sub>2</sub> systems were calculated by using first-principles methods based on density functional theory (DFT). The generalised gradient approximation (GGA) with PBE [29] exchange–correlation functional, as implemented in the VASP package [30,31] was used. The projector augmented

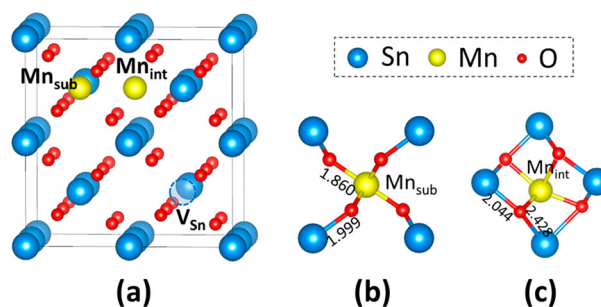


**Figure 1.** (a) Supercell of the Mn-doped SnO<sub>2</sub> with possible defects; partial geometry model of (b) Mn<sub>sub</sub> and (c) Mn<sub>int</sub> in Mn-doped SnO<sub>2</sub>.

wave method [32] was used to represent the ionic cores, and the following electrons were considered as valence: Sn's 5s and 5p; O's 2s and 2p; and Mn's 3d and 4s. Wave functions were represented in a plane-wave basis truncated at 600 eV. Large 3 × 3 × 3 SnO<sub>2</sub> supercells containing 162 atoms and medium 2 × 2 × 2 supercells containing 48 atoms were employed in our DFT calculations to represent low and high doping concentrations. For the Mn substitution (Mn<sub>sub</sub>), one Sn atom has been replaced with one Mn atom, and for Mn interstitial (Mn<sub>int</sub>), one extra Mn atom has been introduced to the supercell, as illustrated in Figure 1(a). The Monkhorst–Pack method was used to generate a regular 10 × 10 × 14 k-point mesh for the Brillouin zone integration. The geometry relaxations were performed with a conjugate-gradient optimiser that varied the volume and shape of the unit cell, and the tolerance imposed on the atomic forces was 0.01 eV·Å<sup>-1</sup>. Hybrid functional corrections (HSE06) have been applied (on top of the PBE-optimised geometries) to improve the estimation of Kohn–Sham bandgap energy. By using these parameters, we obtained total energies that were converged to within 0.5 meV per formula unit.

## Results and discussion

### Possibility of forming interstitials in SnO<sub>2</sub>

In oxide RRAMs, point defects dominate the RS behaviour. Thus, it is necessary to investigate the forming condition for each point defect and defect pair. The formation energies of all possible point defects (including vacancies, substitutions and interstitials) and defect pairs in Mn-doped SnO<sub>2</sub> have been calculated. As illustrated in Figure 1(a), Mn<sub>sub</sub> refers to an Mn atom (yellow) that replaces one Sn atom (grey) and Mn<sub>int</sub> to an Mn atom occupying an interstitial site in the SnO<sub>2</sub> supercell. V<sub>Sn</sub> is the vacancy created by removing one Sn atom. (The illustrated SnO<sub>2</sub> is the supercell of 2 × 2 × 2 containing 48 atoms.) The formation energy of SnO<sub>2</sub> with various defects in the neutral state can be calculated as follow:

$$\Delta E_f = E_{\text{defect}} - E_{\text{supercell}} - \sum N_i \cdot \mu_i$$

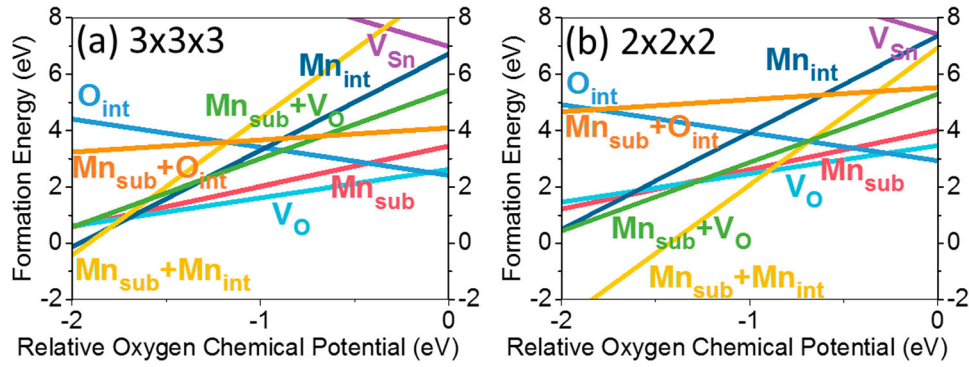


**Figure 2.** Relative oxygen chemical potential dependent formation energy of all possible defects in Mn-doped  $\text{SnO}_2$  of (a)  $3 \times 3 \times 3$  supercell and (b)  $2 \times 2 \times 2$  supercell.

where  $E_{\text{defect}}$  is the total energy of supercell with the specific defects;  $E_{\text{supercell}}$  is the total energy of the pristine  $\text{SnO}_2$  supercell;  $N_i$  is the number of the interstitial atoms that are added into or removed from  $\text{SnO}_2$ , and  $\mu_i$  the relevant chemical potentials of those atoms. For each defect pair, all the possible relative sites have been considered and the one with the lowest energy has been plotted in Figure 2.

In Figure 2(a), the relative oxygen chemical potential dependent defect formation energies in the  $3 \times 3 \times 3$  Mn-doped  $\text{SnO}_2$  supercells have been plotted, which represents a relatively low Mn-doping concentration. Among the intrinsic defects of pristine  $\text{SnO}_2$ , i.e.  $V_{\text{O}}$ ,  $O_{\text{int}}$ , and  $V_{\text{Sn}}$ ,  $V_{\text{O}}$  possesses the lowest formation energy in almost the whole range, while  $O_{\text{int}}$  is only likely to form under Sn-poor/O-rich conditions, which agreed with previous DFT calculations performed with similar methods [33,34] and experimental results [35]. In the Mn-doped  $\text{SnO}_2$ , owing to the high solid solubility of Mn in  $\text{SnO}_2$ , the formation energy of  $\text{Mn}_{\text{sub}}$  is comparable to that of  $V_{\text{O}}$  under O-poor conditions. This suggests that Mn substitutions in  $\text{SnO}_2$  tend to happen under Sn-rich/O-poor conditions. It is noticeable that  $\text{Mn}_{\text{sub}} + \text{Mn}_{\text{int}}$  showed the lowest formation energy in O-poor conditions, followed by  $\text{Mn}_{\text{int}}$ . It implies that  $\text{Mn}_{\text{int}}$  instead of  $V_{\text{O}}$  is highly possible in Sn-rich/O-poor conditions.

In Figure 2(b), the higher Mn-doping concentration has been calculated with a  $2 \times 2 \times 2$  Mn-doped  $\text{SnO}_2$  supercell. The possibility of forming  $\text{Mn}_{\text{int}}$  further increases under Sn-rich/O-poor conditions, as the formation energy differences between  $\text{Mn}_{\text{sub}} + \text{Mn}_{\text{int}}$  pair and other defects increased significantly. This indicates increasing Mn-doping concentration in  $\text{SnO}_2$  can effectively increase the formation possibility of  $\text{Mn}_{\text{int}} + \text{Mn}_{\text{sub}}$  pairs. Hence, to achieve Mn interstitials in experiments, synthesis of Mn-doped  $\text{SnO}_2$  in Sn-rich or O-poor conditions with a higher Mn-doping level is critical, such as via sealed solvothermal methods or annealing in inert gases instead of in the air, etc.

### Multi-level resistive switching and synaptic behaviour under light stimuli with Mn interstitials

It has been confirmed in our previous work that the stable multi-level RS can be observed only in 12.5 mol-% Mn-doped  $\text{SnO}_2$  rather than pure  $\text{SnO}_2$  or lower Mn-doping concentrations [27]. Together with the calculated defect formation energy results in Figure 2 and additional XPS and  $I$ - $V$  characterisations in the ESI, it is reasonable to believe that by increasing the Mn-doping concentration and synthesising the Mn-doped  $\text{SnO}_2$  under Sn-rich/O-poor condition, the formation of Mn interstitials can be significantly improved, which is critical in achieving multi-level RS. To investigate the RS behaviour triggered by Mn interstitials, the Au/Mn- $\text{SnO}_2$ /Au RRAMs have been fabricated for current-voltage ( $I$ - $V$ ) tests. The detailed fabrication methods and characterisations can be found in our previous works [27,28]. The calculated crystal parameter and TEM images of highly self-assembled Mn-doped  $\text{SnO}_2$  nanoparticles are provided in Figure S-3, and the cross-sectional TEM and EDS images are provided in Figure S-4 in the ESI.

It has been reported that the migration energy barrier of cationic interstitial is higher than that of  $V_{\text{O}}$  [12]. Thus, to understand the RS behaviour triggered by  $\text{Mn}_{\text{int}}$  under electrical fields, the current-voltage characteristics have been studied with the voltage sweeping mode of  $0 \rightarrow 3$  (or  $5$ )  $\rightarrow 0 \rightarrow -3$  (or  $-5$ )  $\rightarrow 0$  V. As  $\text{Mn}_{\text{int}}$  can only migrate or be oxidised/deoxidised when the current is high enough. By applying different constant current (CC), the migration of  $\text{Mn}_{\text{int}}$  in Mn-doped  $\text{SnO}_2$  thin film can be regulated. The  $I$ - $V$  curves with different CC applied are provided in Figure 3. It is clearly showing that when the applied CC is too low [CC = 0.0001 A in Figure 3(a)], the thin film cannot be effectively switched, while by increasing the CC to 0.001 A as in Figure 3(b), the film switched from high resistance state (HRS) to lower resistance state at 2.49 V and the response current reached CC immediately. However, due to the limited CC, the film cannot be switched back to HRS effectively. By further

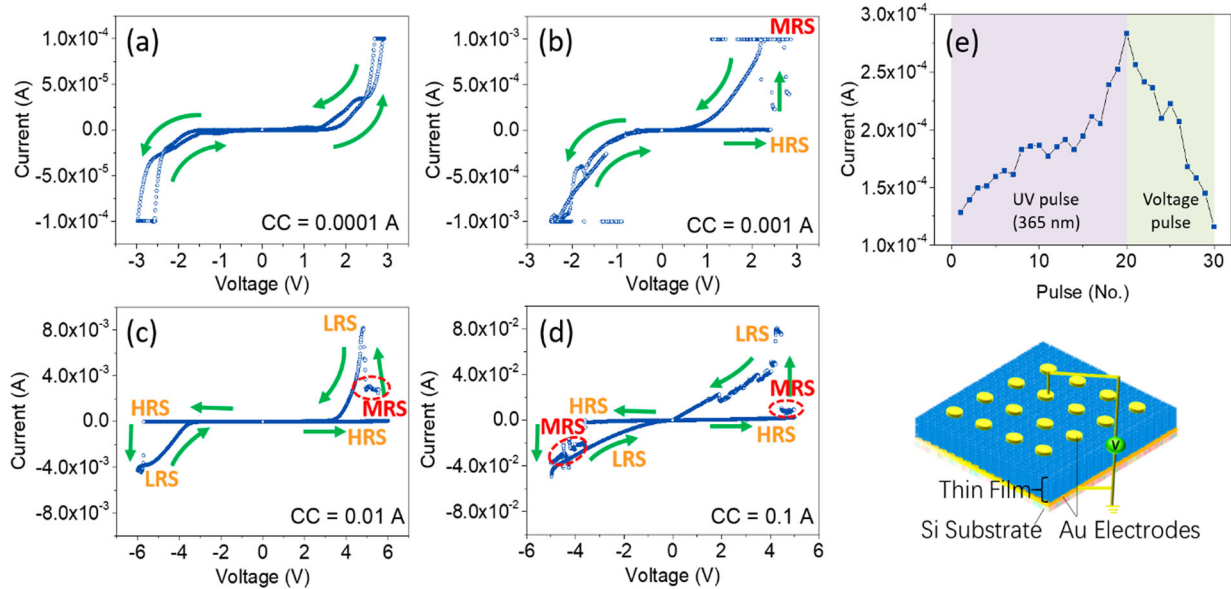


**Figure 3.** (a–d) Voltage–Current measurements of Mn-doped SnO<sub>2</sub> with different constant currents applied; (e) reversible regulation of the conductance by means of 20 UV pulses (SET) and 10 negative voltage pulses (RESET).

increasing the CC to 0.01 A, the intermediate state (MRS) is successfully achieved before the film switched from HRS to LRS and the multi-level RS becomes more obvious when further increasing the CC to 0.1 A as in Figure 3(d). The endurance and retention tests can be found in our previous work [27]. Such  $I$ – $V$  behaviours of Mn-doped SnO<sub>2</sub> indicated the RS relies on the current as well as the applied voltages, which suggests the interstitial Mn in SnO<sub>2</sub> can migrate or be oxidised/deoxidised when the applied voltage or current is high enough. To compare, in Figure S-5 and Ref. [27], no MRS has been observed in the RRAMs of 12.5 mol% Al or In doped SnO<sub>2</sub> where V<sub>O</sub> domains instead of cationic interstitials. Combining the experimental and theoretical investigations above, the critical role of cationic interstitials in achieving multi-state RS can be confirmed.

To understand the mechanism of resistive switching behaviour based on cationic interstitials, the double logarithmic  $I$ – $V$  curves have been provided in Figure 4 with slopes marked. The space charge limited current (SCLC) model gives the best fit to the  $I$ – $V$  curves. More specifically, at the low voltage range, the Ohmic conduction (slope  $\sim 1$ ) is observed when the thermally generated carriers inside the Mn-doped SnO<sub>2</sub> are predominant over the injected charge carrier [36]. Followed by the region fitted with  $I \propto V^2$ , the Ohmic conduction changes to space charge limited (SLC) conduction, when the Ohmic relaxation time is the same as that of carrier transit [37]. With the increase of voltage, the injected carriers domains, as the injected carrier transit time cannot be relaxed by the thermally generated carriers in Mn-doped SnO<sub>2</sub>. It has been confirmed that in the trap-filled limit (TEL) region, where a higher slope (herein,  $> 5$ ) is observed, the existence of traps distributed in the trap-level energies can be ascribed [36].

Such an SCLC model is commonly observed in oxide-based RRAMs with V<sub>O</sub> and active electrode-based RS. However, it is noticeable that the MRS in both Figure 4(c,d) does not follow the SCLC model, and we assume it is the Mn<sub>int</sub> that introduces an extra carrier trap and effectively realised the intermediate resistance states.

In addition, based on the optical (with 2 s pulse width and 365 nm wavelength, read at 0.5 V) SET and voltage pulse (with 1 s pulse width and  $-1$  V voltage) RESET operations, the reversible tuning of memristance has been realised in the Mn-doped SnO<sub>2</sub> memristor, as illustrated in Figure 3(e), while in the pure SnO<sub>2</sub> with only V<sub>O</sub>, the optical SET has not been achieved successfully. The optical SET makes the Mn-doped SnO<sub>2</sub> an ideal optoelectronic memristor material that can respond to UV light directly.

### Electronic and magnetic properties

To further understand the mechanism of multi-level RS and optical SET triggered by Mn<sub>int</sub>, the electronic properties of pure and Mn-doped SnO<sub>2</sub> have been calculated. In this section, only the most stable defects and defect pairs have been considered. The total density of states (TDOS) and projected density of states (PDOS) of pristine SnO<sub>2</sub> and Mn-doped SnO<sub>2</sub> with the possible point defects and defect pairs are illustrated in Figure 5(a–f) and the enlarged DOS around Fermi level are provided in Figure 5(a'–f'). The Fermi level is indicated by dashed lines at the zero-energy level.

The PDOS analysis shows that the valence band (VB) of pristine SnO<sub>2</sub> is mainly composed of oxygen states, while tin contributes more to the conduction band (CB) edge. The introduction of Mn<sub>sub</sub> (Figure

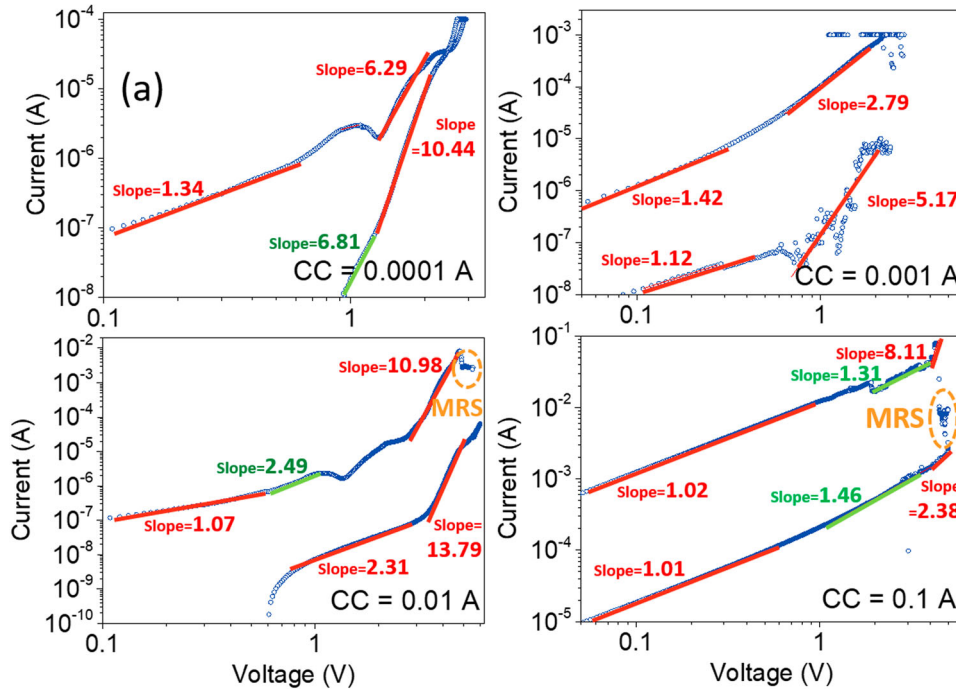


**Figure 4.** Double logarithmic plots of  $I$ - $V$  curves of Mn-doped  $\text{SnO}_2$  with different constant currents applied.

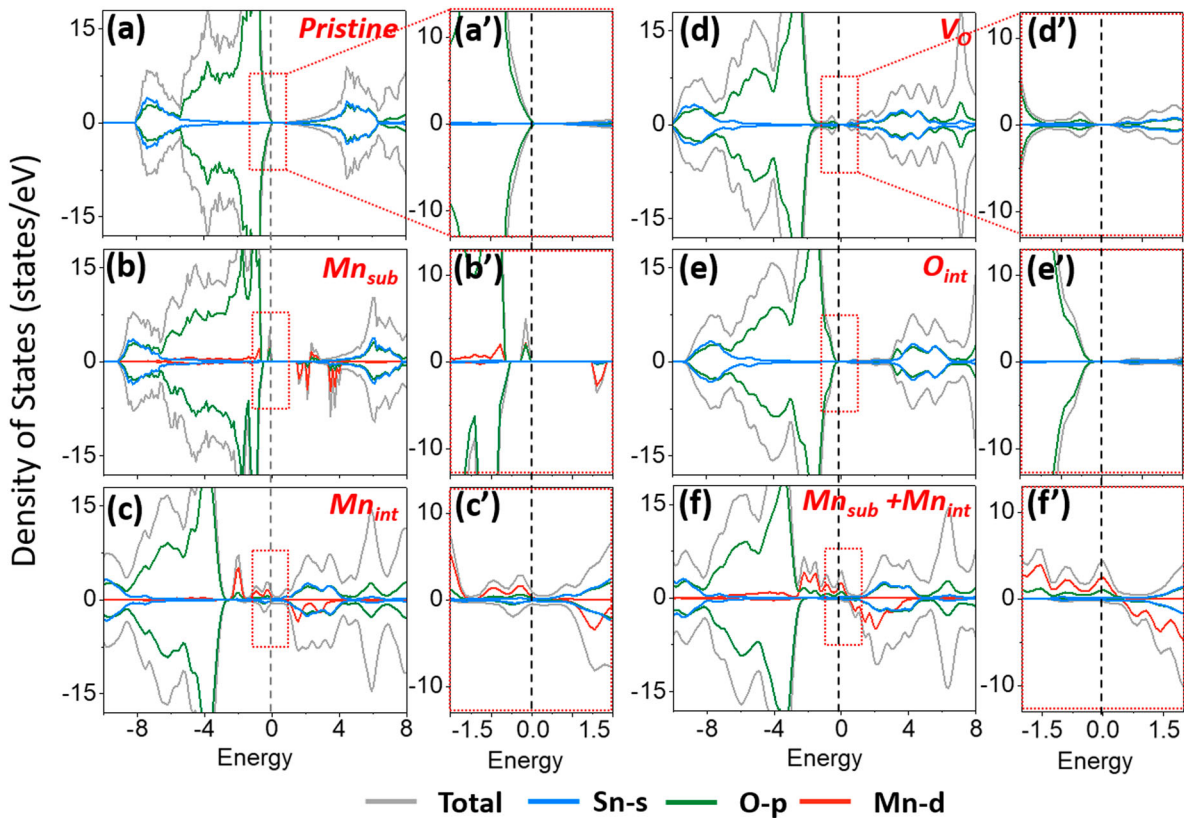


**Figure 5.** Density of states of pristine and Mn-doped  $\text{SnO}_2$  with defects.

5(b)),  $\text{Mn}_{\text{int}}$  (Figure 5(c)) and  $\text{V}_\text{O}$  (Figure 5(d)) generate gap states above the valence band and the Fermi level of  $\text{SnO}_2$  will shift to a higher energy level, while  $\text{O}_{\text{int}}$  (Figure 5(e)) show very little influence on that of  $\text{SnO}_2$ .

In Figure 5(f), the  $\text{Mn}_{\text{sub}} + \text{Mn}_{\text{int}}$  pair, the most possible defect in Mn-doped  $\text{SnO}_2$ , is the only one that

induces an energy band across the Fermi level, which is located just below the CB. From Figure 5(f), it is observed that Mn (d) is the main contributor to the peak, and it leads to overlap with O and Sn above the Fermi level, resulting in an obvious splitting. The raised multiple peaks indicated the traps distributed within the forbidden energy gap, which is assumed the main

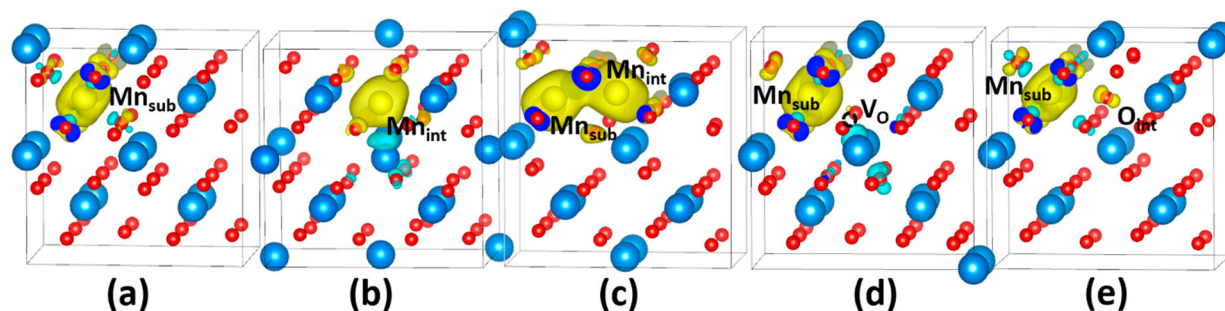


**Figure 6.** Partial charge density for Mn-doped SnO<sub>2</sub> at (a) Mn<sub>sub</sub>; (b) Mn<sub>int</sub>; (c) Mn<sub>sub</sub> + Mn<sub>int</sub> pair; (d) Mn<sub>sub</sub> + V<sub>O</sub> pair and (e) Mn<sub>sub</sub> + O<sub>int</sub> pair.

factor in achieving multi-level RS in experiments as the multiple peaks may provide more electron trapping centres with more energy levels [36]. The raised peaks can also promote the optical SET in the experiments with a relative low light intensity owing to the narrowed bandgap.

Meanwhile, the formation of Mn<sub>int</sub> is also critical in the forming of a conductive path in the RRAM. Compared to the pristine defects in SnO<sub>2</sub>, i.e. V<sub>O</sub> and O<sub>int</sub>. It is noticeable that Mn-doping reduces the bandgap of SnO<sub>2</sub>. The partial charge density for each defect or defect pair has been provided in Figure 6(a–e), in which it is observed that the gap states of both Mn<sub>sub</sub> (Figure 6(a)) and Mn<sub>int</sub> (Figure 6(b)) point defects and Mn<sub>sub</sub> + V<sub>O</sub> (Figure 6(d)) and Mn<sub>sub</sub> + O<sub>int</sub> (Figure 6(e)) defect pairs are localised around Mn<sub>sub</sub>, while only that of the Mn<sub>sub</sub> + Mn<sub>int</sub> pair (Figure 6(c)) spreads over the pairs, which may give an access to form connective paths in the supercell. This also promotes the SET and RESET process in the RRAMs.

## Conclusions

The resistive switching based on the migration of oxygen vacancies from oxides and cations from active electrodes has been intensively studied. However, owing to the high mobility of oxygen vacancies and relative low endurance of cations from electrodes, the performance of memristors has been greatly limited. This paper has systematically studied an alternative defect in metal oxides, the cationic interstitial, which has been overlooked in achieving resistive switching. By investigating the electronic property changes induced by Mn<sub>int</sub> in SnO<sub>2</sub>, the interstitial-induced resistive switching behaviour can be understood. Via first-principle studies, we find that the Mn substitution with Mn interstitial can be formed by synthesizing Mn-doped SnO<sub>2</sub> under Sn-rich/O-poor conditions. The weakly bonded interstitials can significantly change the electrical structures of SnO<sub>2</sub> and raised an intermediate state in the bandgap. This merit allows it to achieve stable multiple resistance states under *I*–*V* sweep and analogue resistive switching under light stimuli. These insights into

the role of cationic interstitials provide inspirations on the rational material design for memristors.

## Disclosure statement

No potential conflict of interest was reported by the author(s).

## Funding

Z. Xu acknowledges financial support from the Beijing Technology and Business University [grant number 19005902140]. P. Guan would like to thank the financial support from the Research Training Program (RTP) funded by the Department of Education, Australia.

## ORCID

Peiyuan Guan  <http://orcid.org/0000-0003-2441-864X>

## References

- [1] Yao P, Wu H, Gao B, et al. Fully hardware-implemented memristor convolutional neural network. *Nature*. 2020; 577:641.
- [2] Strukov DB, Snider GS, Stewart DR, et al. The missing memristor found. *Nature*. 2008;453:80–83.
- [3] Qin Y, Bao H, Wang F, et al. Recent progress on memristive convolutional neural networks for edge intelligence. *Adv Intell Syst*. 2020;2:2000114.
- [4] Magyari-Kope B, Park SG, Lee HD, et al. First principles calculations of oxygen vacancy-ordering effects in resistance change memory materials incorporating binary transition metal oxides. *J Mater Sci*. 2012;47:7498–7514.
- [5] Cheng XF, Xia SG, Hou X, et al. Racemic effect on the performance of organic multilevel memory: beyond molecular design. *Adv Mater Technol*. 2017;2:1700202.
- [6] Chen Z, Huang W, Zhao W, et al. Ultrafast multilevel switching in Au/YIG/n-Si RRAM. *Adv Electron Mater*. 2019;5:1800418.
- [7] Yang C-S, Shang D-S, Chai Y-S, et al. Electrochemical-reaction-induced synaptic plasticity in MoO<sub>x</sub>-based solid state electrochemical cells. *Phys Chem Chem Phys*. 2017;19:4190–4198.
- [8] Zhou L, Yang S, Ding G, et al. Tunable synaptic behavior realized in C<sub>3</sub>N composite based memristor. *Nano Energy*. 2019;58:293–303.
- [9] Nili H, Vincent A, Prezioso M, et al. Comprehensive compact phenomenological modelling of integrated metal-oxide memristors. *IEEE Trans Nanotechnol*. 2020;19:344–349.

- [10] Mohammad B, Jaoude MA, Kumar V, et al. State of the art of metal oxide memristor devices. *Nanotechnol Rev.* **2016**;5:311–329.
- [11] Gjk A, Ms B, Ys B, et al. Mechanism of analog bipolar resistive switching and work function in Au/Na<sub>0.5</sub>Bi<sub>0.5</sub>TiO<sub>3</sub>/Pt heterostructure thin films. *Mater Chem Phys.* **2020**;257:123765.
- [12] Zhu L, Zhou J, Guo Z, et al. Synergistic resistive switching mechanism of oxygen vacancies and metal interstitials in Ta<sub>2</sub>O<sub>5</sub>. *J Phys Chem C.* **2016**;120:2456.
- [13] Chen J, Hsin C-L, Huang C-W, et al. Dynamic evolution of conducting nanofilament in resistive switching memories. *Nano Lett.* **2013**;13:3671.
- [14] Waser R, Dittmann R, Staikov G, et al. Redox-based resistive switching memories—nanoionic mechanisms, prospects. *Adv Mater.* **2009**;21:2632.
- [15] Kamiya K, Yang MY, Magyari-Kpe B, et al. Modeling of resistive random access memory (RRAM) switching mechanisms and memory structures. Woodhead, Cambridge; **2014**. p. 262.
- [16] Xu Z, Guan P, Ji T, et al. Cationic interstitials: an overlooked ionic defect in memristors. *Front Chem.* **2022**;10:944029.
- [17] Gu T, Tada T, Watanabe S, et al. Conductive path formation in the Ta<sub>2</sub>O<sub>5</sub> atomic switch: first-principles analyses. *ACS Nano.* **2010**;4:6477.
- [18] Hussain F, Imran M, Rana AM, et al. An insight into the dopant selection for CeO<sub>2</sub>-based resistive-switching memory system: a DFT and experimental study. *Appl Nanosci.* **2018**;8:839.
- [19] Talukdar A. Structural and electrical characterization of tin oxide resistive switching [PhD dissertation]. University of Texas, El Paso; **2017**.
- [20] Trapatseli M. Doping controlled resistive switching dynamics in transition metal [PhD dissertation]. University of Southampton, Southampton; **2018**.
- [21] Deuermeier J, Kiazadeh A, Klein A, et al. Multi-level cell properties of a bilayer Cu<sub>2</sub>O/Al<sub>2</sub>O<sub>3</sub> resistive switching device. *Nanomater.* **2019**;9:19521.
- [22] Facchetti A, Marks T. *Transparent electronics: from synthesis to applications.* Wiley, Hoboken; **2010**.
- [23] Huang C-H, Huang J-S, Lai C-C, et al. Manipulated transformation of filamentary and homogeneous resistive switching on ZnO thin film memristor with controllable multistate. *ACS Appl Mater Interfaces.* **2013**;5:6017–6023.
- [24] Lin J, Peng Z, Xiang C, et al. Graphene nanoribbon and nanostructured SnO<sub>2</sub> composite anodes for lithium ion batteries. *ACS Nano.* **2013**;7:6001–6006.
- [25] Pan J, Li S, Ou W, et al. The photovoltaic conversion enhancement of NiO/Tm: CeO<sub>2</sub>/SnO<sub>2</sub> transparent pn junction device with dual-functional Tm: CeO<sub>2</sub> quantum dots. *Chem Eng J.* **2020**;393:124802.
- [26] Hao D, Liu D, Shen Y, et al. Air-stable self-powered photodetectors based on lead-free CsBi<sub>3</sub>I<sub>10</sub>/SnO<sub>2</sub> heterojunction for weak light detection. *Adv Funct Mater.* **2021**;31:2100773.
- [27] Xu Z, Younis A, Cazorla C, et al. Engineering cationic defects in transparent tin oxide superlattices. *Mater Des.* **2018**;155:71.
- [28] Xu Z, Guan P, Younis A, et al. Manipulating resistive states in oxide based resistive memories through defective layers design. *RSC Adv.* **2017**;7:56390.
- [29] Perdew JP, Burke K, Ernzerhof M. Generalized gradient approximation made simple. *Phys Rev Lett.* **1996**;77:3865.
- [30] Kresse G, Furthmüller J. Efficient iterative schemes for ab initio total-energy calculations using a plane-wave basis set. *Phys Rev B.* **1996**;54:11169.
- [31] Kresse G, Joubert D. From ultrasoft pseudopotentials to the projector augmented-wave method. *Phys Rev B.* **1999**;59:1758.
- [32] Blöchl PE. Projector augmented-wave method. *Phys Rev B.* **1994**;50:17953.
- [33] Bma B, Ns A, Mra A, et al. Fe-doped SnO<sub>2</sub> transparent semi-conducting thin films deposited by spray pyrolysis technique: thermoelectric and p-type conductivity properties. *Solid State Sci.* **2009**;11:233–239.
- [34] He H, Xie Z, Li Q, et al. On the possibility of p-type doping of SnO<sub>2</sub> with Mg: A first-principles study. *Comput Mater Sci.* **2015**;101:62–65.
- [35] Mehraj S, Shahnawaze Ansari M, Al-Ghamdi AA, et al. Annealing dependent oxygen vacancies in SnO<sub>2</sub> nanoparticles: structural, electrical and their ferromagnetic behavior. *Mater Chem Phys.* **2016**;171:109–118.
- [36] Shang DS, Wang Q, Chen LD, et al. Effect of carrier trapping on the hysteretic current-voltage characteristics in Ag/La<sub>0.7</sub>Ca<sub>0.3</sub>MnO<sub>3</sub>/Pt heterostructures. *Phys Rev B.* **2006**;73:24.
- [37] Kao WHKC. *Electrical transport in solids, with particular reference to organic semiconductors.* Oxford: Pergamon Press; **1981**. p. 660.